Author Manuscript

Author Manuscript

Author Manuscript

Author Manuscript

HHS Public Access

Author manuscript

J Biomed Mater Res A. Author manuscript; available in PMC 2023 September 28.

Published in final edited form as:

J Biomed Mater Res A. 2023 September ; 111(9): 1372–1378. doi:10.1002/jbm.a.37539.

Alpha-ketoglutaric acid based polymeric particles for cutaneous wound healing

Madhan M. C. S. Jaggarapu[1], **Deepanjan Ghosh**[2], **Tyler Johnston**[3], **Jordan R. Yaron**[1], **Joslyn L. Mangal**[3], **Sahil Inamdar**[1], **Mallikarjun Gosangi**[1], **Kaushal Rege**[1,2,4,5,6], **Abhinav P. Acharya**[1,2,4,5,6,7]

[1]Chemical Engineering, School for the Engineering of Matter, Transport, and Energy, Arizona State University, Tempe, Arizona 85281, USA

[2]Biological Design, School for the Engineering of Matter, Transport, and Energy, Arizona State University, Tempe, Arizona 85281, USA

[3]Molecular Biosciences and Biotechnology, The College of Liberal Arts and Sciences, School of Life Sciences, Arizona State University, Tempe, Arizona 85281, USA

[4]Biomedical Engineering, School of Biological and Health Systems Engineering, Arizona State University, Tempe, Arizona 85281, USA

[5]Materials Science and Engineering, School for the Engineering of Matter, Transport, and Energy, Arizona State University, Tempe, Arizona 85281, USA

[6]Biodesign Center for Biomaterials Innovation and Translation, Arizona State University, Tempe, Arizona 85281, USA

[7]Biodesign Center for Immunotherapy, Vaccines and Virotherapy, Arizona State University, Tempe, Arizona 85281, USA

Abstract

Metabolites are not only involved in energy pathways but can also act as signaling molecules. Herein, we demonstrate that polyesters of alpha-ketoglutararte (paKG) can be generated by reacting aKG with aliphatic diols of different lengths, which release aKG in a sustained manner. paKG polymer-based microparticles generated via emulsion-evaporation technique lead to faster keratinocyte wound closures in a scratch assay test. Moreover, paKG microparticles also led to faster wound healing responses in an excisional wound model in live mice. Overall, this study shows that paKG MPs that release aKG in a sustained manner can be used to develop regenerative therapeutic responses.

Correspondence: Abhinav P. Acharya, Chemical Engineering, School for the Engineering of Matter, Transport, and Energy, Arizona State University, Tempe, Arizona 85281, USA. abhi.acharya@asu.edu.

AUTHOR CONTRIBUTIONS

Madhan M. C. S. Jaggarapu, Tyler Johnston, Joslyn L. Mangal, Sahil Inamdar, Mallikarjun Gosangi, Jordan R. Yaron and Deepanjan Ghosh performed investigations and designed experiments. Kaushal Rege and Abhinav P. Acharya provided funds and supervised studies.

CONFLICT OF INTEREST STATEMENT

Kaushal Rege is affiliated with Synergyan, LLC, Abhinav P. Acharya is affiliated with Immunometabolix LLC and VaderBio LLC, Jordan R. Yaron is affiliated with Vivo Bioconsulting, LLC.

Author Manuscript Author Manuscript Author Manuscript Author Manuscript

Keywords

alpha-ketoglutarate; metabolism; microparticle; TCA cycle; wound healing

1 | INTRODUCTION

Metabolites have emerged as essential factors in reprograming the immune system.[1–3] Specifically, metabolites are defined as the intermediate biochemical materials of catabolic and anabolic processes.[4] They play a critical role in building cellular components and cell growth.[5] The use of metabolites in reprogramming the immune system has led to new fields of study that focus on understanding the role of metabolism in several diseases including cancer, autoimmune disorders, and Alzheimer's among others.[6–8] Recent studies have brought to light roles of several metabolites in modulating the immune system such as 2-hydroxyglutarate, 2-deoxyglucose among others.[9,10] Alpha-ketoglutarate (aKG) is a key metabolite in the Krebs cycle and is being actively studied because of its several beneficiary roles.[11] Importantly, the overall rate of the Krebs cycle is determined by the generation of aKG. aKG has been shown to play an active role in multiple cellular metabolism and helps in maintaining the nitrogen balance.[12] Recent findings show the role of aKG in inducing protective immune responses.[13] Most of the aKG related studies are conducted in the field of cancer, regenerative medicine and cellular metabolism[14,15] and its role in injury and wound healing has yet to be elucidated.

Skin injury is common at any stage of life and wound healing is a complex physiological process with a myriad of cellular events.[16] Efficient wound healing is important for maintaining critical defense mechanism of skin by restoring the integrity of the injured tissue.[17] Dysregulation of wound healing may result in chronic wounds, which can further lead to tissue necrosis and systemic infection. Thus, wound healing plays a critical role in maintaining the homeostasis of the immune system in patients with surgical wounds or traumatic injuries.[18,19] Fabricating a functional material as a delivery system provides integrated functions for wound healing. Biomaterials such as lipid-based particles, polymeric particles, and hydrogels have been using for wound healing in pre-clinical settings.[20,21] Notably, the landscape of polymeric materials has made a huge impact in wound healing research, as evident by applications in past 20 years.[22,23] Adhesion and phagocytosis of polymeric particles by the phagocytic cells at the region of injury or the wound help in healing. In this study, we utilized aKG metabolite to generate polymeric particles, which can enhance this healing process.

2 | RESULTS AND DISCUSSIONS

Since small molecule metabolites such as aKG have high diffusion kinetics, they need to be given in high and frequent dosages to achieve the desired effect in vivo.[24] Additionally, injections of aKG alone will cause fast diffusion and elimination from body. Thus, to overcome the high diffusion of aKG out from the application site, we generated polymers with aKG in their backbone, which can release aKG in a sustained manner to maximize the utilization of aKG in the cell or tissue. For the polymer synthesis, aKG was reacted with

Author Manuscript Author Manuscript Author Manuscript Author Manuscript

1,8-Octanediol, or 1,10-Decanediol, or 1,12-Dodecanediol to get polymers 1,8-paKG, 1,10-paKG, and 1,12-paKG. All the paKG polymers were prepared by using an esterification procedure by heating mixture of acid and alcohol at 130°C for 24 h under vacuum (Figure 1A). ^{1}H NMR spectrum was used to assess the degree of modification of acid to ester group (Figure 1B). No peak of acid group at the range of 10–12 ppm demonstrated that the ester was formed in all polymers. Moreover, FTIR also confirmed that the polymers were generated (Figure 1C), as no acid broad peak at 3100 cm^{-1} and carbonyl peak around 1650 cm^{-1} were observed. paKG polymers can be immunosuppressive, and by feeding directly into the Krebs cycle might modulate metabolism of different cell types.[2,25] Notably, polymers with 1,8-Octanediol, or 1,10-Decanediol, or 1,12-Dodecanediol might impart different properties to the polymers including solubility, biodegradability, hydrophobicity and ability to generate particles. In fact, it has been demonstrated using different metabolites such as fumarate, and succinate that different diol based monomers modulate the polymer characteristics, which can be exploited for biological applications.[26,27]

Synthesized paKG polymers were utilized to generate microparticles by using a previously reported method.[3] In brief, the polymers were dissolved in dichloromethane (DCM) and this organic mixture was then added to polyvinyl alcohol (PVA) solution in deionized H_2O followed by immediate homogenization. The formed emulsion was then added to 1% PVA solution and stirred for 3 h to evaporate DCM.[28–30] The particles thus formed were then washed 3 times with deionized H_2O by centrifuging to remove excess PVA. The generated particles were then freeze-dried and used for further studies. To determine the size of the 1,10- paKG microparticles, dynamic light scattering was utilized, which showed that the size of the particles before lyophilization was 3074 ± 187 nm, whereas after lyophilization the size was 3890 ± 388 nm. Since these, before and after lyophilization sizes were found to be similar these data suggest that the size of the microparticles is not altered after freeze-drying process.

To test if different MPs could release aKG in a sustained manner, release kinetics experiments in pH 7.4 (1x PBS, physiological pH) were performed. Amount of aKG released at different time points was determined using high-performance liquid chromatography (HPLC). The release kinetics study demonstrates that all the four paKG MPs released aKG in a sustained fashion for more than a week. Release of metabolites for 10-days was determined since, several in vitro scratch assay tests and in vivo mice experiments for acute wound healing have a similar time frame.[31,32]

Immunosuppression has been shown to accelerate wound healing.[33] All the three paKG MPs showed a similar type of release kinetics (Figure 2A) but we have previously demonstrated that 1,10 paKG MPs can lead to immunosuppression,[3] and therefore in this study we tested if these can lead to faster wound healing. First, monolayers of serum-starved (i.e., proliferation-arrested) human keratinocytes (HaCaT) cells were cultured and used for the cell migration scratch assay test with 1,10 paKG MPs. The results demonstrated that as compared to the monomers of 1,10 decanediol, and aKG; 1,10 paKG MPs were able to allow for higher cell migration. TGF-beta (TGFb, 2 ng/mL) was used as a positive control, in these experiments (Figure 2B). HaCaT cells are frequently utilized to test the wound closure in a scratch assay. Several small molecules, proteins, peptides, and RNA/DNA have

Author Manuscript Author Manuscript Author Manuscript Author Manuscript

been utilized to test the wound closure rate.[34–40] 40 paKG MPs led to only 40% of wound closure, as compared to the post to control off 80%. This potentially is due to slow release of aKG from paKG particles. Moreover, for this specific test, the paKG particles by themselves may not be enough to accelerate wound closures, and other modalities might be required in combination to be equivalent to the positive control. However, we have previously demonstrated that paKG MPs can modulate immune responses, and since wound healing is affected by immune cells, the potential of paKG MPs by themselves in a cutaneous wound mouse model was tested. Full-thickness splinted cutaneous wounds were created in BALB/c mice (Figure 2C) and paKG MPs or saline or soluble aKG were applied on top of the wound on day 0, in addition to a Tegaderm dressing. Wound closure was observed for 10 days by taking photographs and by planimetrically determining the wound area measurements with ImageJ/FIJI (Figures 2D and 3A). Ultimate tensile strength studies were also performed on the skin to determine the strength of the healed skin. The ultimate tensile strength was significantly higher in the 1,10-paKG MPs group as compared to the saline control (Figure 3B). Importantly, it was observed that the wounds closed at day 9 in 1,10-paKG MPs group, which was significantly faster as compared to soluble aKG or saline. Interestingly, it was observed that the paKG MPs treated wound sites increased collagen type III deposition as observed by picrosirius staining of the wound bed (Figure 3C). Moreover, qualitatively, it was observed that there was fewer cell infiltration in paKG MPs condition as compared to the PBS and soluble aKG treatment groups in the wound bed (Figure 3D).

To our knowledge, this is the first study, which demonstrates that one-time application of aKG metabolite-based polymers can lead to significant modulation of wound closure. The advent of biomaterial usage in the field of drug delivery has resulted in increased attention in the field of biomedicine and bioengineering fields. Herein, we used a delivery system which itself can be used to stimulate the healing process of wound by releasing a metabolite.

In a cutaneous wound, distress to the upper layer of the skin, the epidermis, can trigger a series of cellular responses that involve the recruitment of immune cells to the wound bed.[41] Specifically, innate immune cells such neutrophils, and macrophages, prevent pathogens from entering the wound bed.[42] Following the inflammatory phase, the wound bed undergoes a phase of remodeling and repair.[43] Interestingly, although growth factors act during the remodeling and repair phase to improve wound healing kinetics, these do not directly modulate the inflammatory or anti-inflammatory phase of the wound healing process and therefore, are known to be sub-optimal.[44,45] The data presented herein demonstrate that 1,10-paKG MPs might assist the wound closure by accelerating the cell proliferation phase and potentially allowing for the pro-inflammatory phase to occur by releasing low-levels of aKG in a sustained manner. In contrast, the cutaneous wounds that were exposed to soluble aKG, received aKG in a bolus manner, leading to immediate immune suppression and, thereby, suppressing the inflammatory phase of wound healing. Hence, soluble aKG might prohibit professional phagocytes from eliminating pathogens in the wound bed, while the sustained release of aKG from the 1,10-paKG MPs still allowed for the inflammatory phase to occur but potentially accelerated the remodeling phase. In vitro soluble aKG directly acts on the HaCaT cells and since there is no immune cells involved aKG assists in closure of the wound.

Author Manuscript Author Manuscript Author Manuscript Author Manuscript

3 | CONCLUSION

In summary, metabolite-based polymers provide a new technique to deliver metabolites locally to modulate the proliferation of cells. Importantly, 1,10-paKG MPs were able to provide accelerated wound closure responses in vivo by allowing for different phases of wound healing to occur.

4 | METHODS

4.1 | Polymer synthesis

Ketoglutaric acid (1 g, 5.56 mmol) and diols (0.811 g, 5.56 mmol for 1,8 octanediol; 0.97 g, 5.56 mmol for 1,10 decanediol; and 1.124 g, 5.56 mmol for 1,12 dodecanediol) were mixed at equimolar ratio in a round-bottom flask without any solvent. This mixture was stirred at 130°C for 48 h under nitrogen. The polymer thus generated was precipitated in methanol solution. Methanol was then evaporated off using a rotary evaporator, and the polymers were then dried under vacuum at room temperature for 48 h.

4.2 | Microparticle synthesis and characterization

paKG polymers were utilized to generate microparticles using an oil-in-water emulsion using solvent evaporation method. In order to generate microparticles, first, 50 mg of the polymers were dissolved in 1 mL of dichloromethane (DCM). This solution was then added to 10 mL of 2% polyvinyl alcohol (PVA) solution in DIH_2O and homogenized at 30,000 rpm using a handheld homogenizer for 2 min. This emulsion was then added to 50 mL of 1% PVA solution and stirred at 400 rpm for 3 h to remove DCM. The particles thus formed were then washed 3 times by centrifuging at 2000 × Gs for 5 min (Eppendorf, Hauppauge, NY), removing the supernatant, and resuspending in DIH_2O. These particles were then freeze dried and used for next experiments. Release kinetics of the metabolites was determined by incubating 1 mg of the microparticles in 1 mL of phosphate buffered saline (PBS) and placed on a rotator at 37°C. Next, triplicates of each release sample were centrifuged at 2000 × Gs for 5 min. After centrifugation, 800 μL of the supernatant was removed and placed into a 1.5 mL tube (Eppendorf, Hauppauge, NY) and then replaced by 800 μL of new buffer. The amount of metabolite released was then determined by developing a new method in a high-performance liquid chromatograph (HPLC, Agilent Technologies, Santa Clara, CA). Specifically, the mobile phase of 0.02 M H_2SO_4 in water was used. A 50 μL of injection volume was utilized in a Hi-Plex H, 7.7 × 300 mm^2, 8 μm column. The flow rate of 1.2 mL/min was utilized and the absorbance was determined using a UV detector at 210 nm. The area under the curve was determined using the ChemStation analysis software as per manufacturer's directions.

4.3 | Animals, wound model, and treatment

The Animal Care Committee of Arizona State University approved all animal studies pertaining to wound healing. Equal numbers of male and female mice were used in strict accordance with the Guide for the Care and Use of Laboratory Animals of the National Institutes of Health. 8-week-old BALB/c mice (strain code 028 – Charles River Laboratories) were anesthetized with 120 mg/kg ketamine and 6 mg/kg xylazine by

Author Manuscript Author Manuscript Author Manuscript Author Manuscript

intraperitoneal injection prior to wounding. The dorsal surface was shaved with an electric clipper and prepped using chlorhexidine gluconate and alcohol swabbing in series on the surgical site. Five-millimeter biopsy punches (Integra Miltex, VWR) were used to create middorsal full-thickness wounds by excising epidermis and dermis, including the panniculus carnosus. Immediately after the surgery on day 0, the wounds were topically treated with 10 μL of PBS containing 1 mg of soluble aKG, 2 mg of paKG MPs, or no microparticle control. A donut-shaped splint with an inner diameter of 6-mm prepared from a 0.5 mm-thick silicone sheet (Grace Bio-Laboratories, Bend, OR) and covered on one side with Tegaderm (3 M) was placed so that the wound was centered within the splint. An immediate-bonding adhesive (Krazy Glue®; Elmer's Inc.) was used to fix the splint to the skin followed by interrupted 4–0 nylon sutures (Monosof™ monofilament nylon sutures, Medtronic) to ensure position. In order to prevent contraction of the wounds, silicon splint was used allowing wounds to heal through granulation and re-epithelialization. The mice were recovered on a heating pad until fully mobile. The mice were housed individually to prevent splint removal.

4.4 | Wound area image analysis

Each wound site was digitally photographed everyday post-wounding, and wound areas were determined on photographs using ImageJ (NIH). Day 0 wound areas were considered as 1 and all wound areas of subsequent days were normalized accordingly. Changes in wound areas were expressed as the proportion of the initial wound areas. All wound area measurements and plots are displayed as mean ± standard error of mean (SEM) from six independent experiments ($n = 6$). The data obtained for each day for each individual mouse was normalized to day 0, then statistics was performed on the normalized data.

4.5 | Ultimate tensile strength measurements

Rectangular sections of the skin around the wound area (20 × 0.5 mm^2, measured by calipers after underlying fascia removal) were excised at days 10 post wounding. Skin samples were stretched until failure at a rate of 2 mm/s using a TA.*XT* Plus texture analyzer. Ultimate tensile strength (UTS) was determined from the maximum force of the tissue prior to failure, where the maximum force (F) and area of the tissue sample (A) determined the ultimate tensile strength (σ, kPa) of the sutured skin ($\sigma = F/A$). The tensile strength of intact skin (with no incision) was also tested for comparison. All tensile strengths are displayed as mean ± standard error of mean (SEM) from four independent experiments ($n = 4$). Tensile strength recovery for skin samples were calculated as a difference between ultimate tensile strength for each group after healing from native skin strength, with the difference then converted to a percentage.

4.6 | H&E and picrosirius staining

Tissue slices were generated for wound area based on previous protocols,[46] and adapted for skin tissue. Briefly, after euthanasia, the skin tissue around the wound bed was dissected fixed in 4% paraformaldehyde, and paraffin embedded. These tissues were then precision cut and mounted on microscope slides for H&E staining. Images of the tissue slices were obtained using a Discover ECHO microscope (San Diego, CA).

Author Manuscript Author Manuscript Author Manuscript Author Manuscript

Picrosirius red stain was achieved by staining the 8 μm sections with 0.1% picrosirius red (Direct Red80, Sigma–Aldrich) and counterstained with Weigert's hematoxylin to reveal fibrillar collagen. The images of the sections were then obtained by capturing the polarizer oriented parallel and orthogonal to each other, which maintain the lamp brightness, condenser opening, objective, zoom, exposure time, and gain parameters constant.

4.7 | Statistical analysis

Data are expressed as mean ± standard error. Comparison between two groups was performed using Student's t test (Microsoft, Excel). Comparisons between multiple treatment groups were performed using one-way ANOVA, followed by Bonferroni multiple comparisons, and $p \leq .05$ was considered statistically significant. Statistical tests were performed using GraphPad Prism Software 6.0 (San Diego, CA).

ACKNOWLEDGMENTS

Kaushal Rege is grateful to the National Institutes of Health (NIH R01 AR074627) for facilitating this research. Jordan R. Yaron would like to acknowledge NIH K01 EB031984 for partial support. Abhinav P. Acharya was supported through NIH R01 AI155907-01, R01AR078343-01, NIH/NSF R01GM144966-01 and NSF AWARD # 2145877. The authors would like to thank Jacquelyn Kilbourne, Dr. Juliane Dagget-Vondras, and Kenneth Lowe for their invaluable technical assistance with in vivo experiments.

Funding information

National Institutes of Health, Grant/Award Numbers: 2145877, NIH/NSF R01GM144966–01, R01AR078343-01, NIH R01 AI155907-01, NIH K01 EB031984, NIH R01 AR074627

DATA AVAILABILITY STATEMENT

The data that support the findings of this study are available from the corresponding author upon reasonable request.

REFERENCES

1. Mangal JL, Inamdar S, Suresh AP, et al. Short term, low dose alpha-ketoglutarate based polymeric nanoparticles with methotrexate reverse rheumatoid arthritis symptoms in mice and modulate T helper cell responses. Biomater Sci. 2022;10:6688–6697. [PubMed: 36190458]
2. Mangal JL, Inamdar S, Le T, et al. Inhibition of glycolysis in the presence of antigen generates suppressive antigen-specific responses and restrains rheumatoid arthritis in mice. Biomaterials. 2021;277:121079. [PubMed: 34454372]
3. Mangal JL, Inamdar S, Yang Y, et al. Metabolite releasing polymers control dendritic cell function by modulating their energy metabolism. J mater chem B. R Soc Chem 2020;8:5195–5203.
4. Baghel R, Maan K, Haritwal T, Rana P. Chapter 2 - integration of epigenomics and metabolomics: from biomarkers discovery to personalized medicine. In: Agrawala PK, Rana P, eds. Epigenetics Metabolomics. Academic Press; 2021 [cited 2022 Dec 15]. Available from: https://www.sciencedirect.com/science/article/pii/B9780323856522000026
5. Figlia G, Willnow P, Teleman AA. Metabolites regulate cell signaling and growth via covalent modification of proteins. Dev Cell. 2020;54: 156–170. [PubMed: 32693055]
6. Assmann N, O'Brien KL, Donnelly RP, et al. Srebp-controlled glucose metabolism is essential for NK cell functional responses. Nat Immunol. 2017;18:1197–1206. [PubMed: 28920951]
7. O'Neill LAJ, Pearce EJ. Immunometabolism governs dendritic cell and macrophage function. J Exp Med. 2015;213:15–23. [PubMed: 26694970]

Author Manuscript Author Manuscript Author Manuscript Author Manuscript

8. Steed AL, Christophi GP, Kaiko GE, et al. The microbial metabolite desaminotyrosine protects from influenza through type I interferon. Science. 2017;357:498–502. [PubMed: 28774928]
9. Abboud G, Choi S-C, Kanda N, Zeumer-Spataro L, Roopenian DC, Morel L. Inhibition of glycolysis reduces disease severity in an autoimmune model of rheumatoid arthritis. Front Immunol. 2018;9:1973. [PubMed: 30233578]
10. Liu P-S, Wang H, Li X, et al. α-Ketoglutarate orchestrates macrophage activation through metabolic and epigenetic reprogramming. Nat Immunol Nat Publ Group. 2017;18:985–994.
11. Rhoads TW, Anderson RM. Alpha-ketoglutarate, the metabolite that regulates aging in mice. Cell Metab. 2020;32:323–325. [PubMed: 32877686]
12. Wu N, Yang M, Gaur U, Xu H, Yao Y, Li D. Alpha-ketoglutarate: physiological functions and applications. Biomol Ther. 2016;24:1–8.
13. Liu S, Yang J, Wu Z. The regulatory role of α-ketoglutarate metabolism in macrophages. Mediators Inflamm. 2021;2021:5577577. [PubMed: 33859536]
14. Chung H-Y, Park YK. Rationale, feasibility and acceptability of ketogenic diet for cancer treatment. J Cancer Prev. 2017;22:127–134. [PubMed: 29018777]
15. Hopkins BD, Pauli C, Du X, et al. Suppression of insulin feedback enhances the efficacy of PI3K inhibitors. Nature. 2018;560:499–503. [PubMed: 30051890]
16. Rodrigues M, Kosaric N, Bonham CA, Gurtner GC. Wound healing: a cellular perspective. Physiol Rev Am Physiol Soc. 2019;99:665–706.
17. Avishai E, Yeghiazaryan K, Golubnitschaja O. Impaired wound healing: facts and hypotheses for multi-professional considerations in predictive, preventive and personalised medicine. EPMA J. 2017;8:23–33. [PubMed: 28620441]
18. Eming SA, Martin P, Tomic-Canic M. Wound repair and regeneration: mechanisms, signaling, and translation. Sci Transl Med. 2014;6:265sr6. [PubMed: 25473038]
19. Eming SA, Krieg T, Davidson JM. Inflammation in wound repair: molecular and cellular mechanisms. J Invest Dermatol. 2007;127:514–525. [PubMed: 17299434]
20. Chen L, Pan Z, Zhu J, Mao Y, Sun J. Novel fabrication of dual nanoparticle loaded-co-polymeric dressing for effective healing efficiency in wound care after fracture surgery. J Biomater Sci Polym ed. 2021;32:2009–2027. [PubMed: 34338145]
21. El-Aassar MR, El-Beheri NG, Agwa MM, et al. Antibiotic-free combinational hyaluronic acid blend nanofibers for wound healing enhancement. Int J Biol Macromol. 2021;167:1552–1563. [PubMed: 33212109]
22. Ali Khan Z, Jamil S, Akhtar A, Mustehsan Bashir M, Yar M. Chitosan Based Hybrid Materials Used for Wound Healing Applications- A Short Review. Vol 69. Int J Polym Mater Polym Biomater. Taylor & Francis; 2020:419–436.
23. Stratton S, Shelke NB, Hoshino K, Rudraiah S, Kumbar SG. Bioactive polymeric scaffolds for tissue engineering. Bioact Mater. 2016;1:93–108. [PubMed: 28653043]
24. Sun K, Tang Y, Li Q, et al. In vivo dynamic monitoring of small molecules with implantable polymer-dot transducer. ACS Nano. 2016;10:6769–6781. [PubMed: 27303785]
25. Acharya AP, Carstens MR, Lewis JS, et al. A cell-based microarray to investigate combinatorial effects of microparticle-encapsulated adjuvants on dendritic cell activation. J Mater Chem B. 2016;4:1672–1685. [PubMed: 26985393]
26. Tatara AM, Watson E, Satish T, et al. Synthesis and characterization of diol-based unsaturated polyesters: poly(diol fumarate) and poly(diol fumarate- *co* -succinate). Biomacromolecules. 2017;18:1724–1735. [PubMed: 28486802]
27. Weinland DH, van der Maas K, Wang Y, et al. Overcoming the low reactivity of biobased, secondary diols in polyester synthesis. Nat Commun. 2022;13:7370. [PubMed: 36450717]
28. Acharya AP, Clare-Salzler MJ, Keselowsky BG. A high-throughput microparticle microarray platform for dendritic cell-targeting vaccines. Biomaterials. 2009;30:4168–4177. [PubMed: 19477505]
29. Acharya AP, Lewis JS, Keselowsky BG. Combinatorial co-encapsulation of hydrophobic molecules in poly(lactide-co-glycolide) microparticles. Biomaterials. 2013;34:3422–3430. [PubMed: 23375950]

Author Manuscript Author Manuscript Author Manuscript Author Manuscript

30. Acharya AP, Sinha M, Ratay ML, et al. Localized multi-component delivery platform generates local and systemic anti-tumor immunity. Adv Funct Mater. 2017;27:1604366.
31. Ghosh D, Salinas CM, Pallod S, et al. Temporal evaluation of efficacy and quality of tissue repair upon laser-activated sealing. Bioeng Transl Med. 2023;8(2):e10412. [PubMed: 36925709]
32. Ridha I, Basiri A, Godeshala S, et al. Chromophore-free sealing and repair of soft tissues using mid-infrared light-activated biosealants. Adv Funct Mater. 2021;31:2007811.
33. Bootun R Effects of immunosuppressive therapy on wound healing. Int Wound J. 2013;10:98–104. [PubMed: 22364410]
34. Kang CW, Han YE, Kim J, Oh JH, Cho YH, Lee EJ. 4-hydroxybenzaldehyde accelerates acute wound healing through activation of focal adhesion signalling in keratinocytes. Sci Rep. 2017;7:14192. [PubMed: 29079748]
35. Su L, Fu L, Li X, et al. Loss of CAR promotes migration and proliferation of HaCaT cells and accelerates wound healing in rats via Src-p38 MAPK pathway. Sci Rep. 2016;6:19735. [PubMed: 26804208]
36. Carretero M, Escámez MJ, García M, et al. In vitro and In vivo wound healing-promoting activities of human cathelicidin LL-37. J Invest Dermatol. 2008;128:223–236. [PubMed: 17805349]
37. Chang L, Liang J, Xia X, Chen X. miRNA-126 enhances viability, colony formation, and migration of keratinocytes HaCaT cells by regulating PI3 K/AKT signaling pathway: miRNA-126 promotes skin wound healing. Cell Biol Int. 2019;43:182–191. [PubMed: 30571843]
38. Saporito P, Vang Mouritzen M, Løbner-Olesen A, Jenssen H. LL-37 fragments have antimicrobial activity against *Staphylococcus epidermidis* biofilms and wound healing potential in HaCaT cell line. J Pept Sci. 2018;24:e3080. [PubMed: 29737589]
39. Kim MK, Choi YC, Cho SH, Choi JS, Cho YW. The antioxidant effect of small extracellular vesicles derived from Aloe vera peels for wound healing. Tissue Eng Regen Med. 2021;18:561–571. [PubMed: 34313971]
40. Büth H, Luigi Buttigieg P, Ostafe R, et al. Cathepsin B is essential for regeneration of scratch-wounded normal human epidermal keratinocytes. Eur J Cell Biol. 2007;86:747–761. [PubMed: 17651862]
41. Wilkinson HN, Hardman MJ. Wound healing: cellular mechanisms and pathological outcomes. Open Biol. 2020;10:200223. [PubMed: 32993416]
42. Keyes BE, Liu S, Asare A, et al. Impaired epidermal to dendritic T cell signaling slows wound repair in aged skin. Cell. 2016;167:1323–1338. [PubMed: 27863246]
43. Ellis S, Lin EJ, Tartar D. Immunology of wound healing. Curr Dermatol Rep. 2018;7:350–358. [PubMed: 30524911]
44. Olekson MAP, Faulknor R, Bandekar A, Sempkowski M, Hsia HC, Berthiaume F. SDF-1 liposomes promote sustained cell proliferation in mouse diabetic wounds. Wound Repair Regen. 2015;23:711–723. [PubMed: 26110250]
45. Yeboah A, Maguire T, Schloss R, Berthiaume F, Yarmush ML. Stromal cell-derived growth Factor-1 alpha-elastin like peptide fusion protein promotes cell migration and revascularization of experimental wounds in diabetic mice. Adv Wound Care. 2017;6:10–22.
46. Acharya AP, Tang Y, Bertero T, et al. Simultaneous pharmacologic inhibition of yes-associated protein 1 and glutaminase 1 via inhaled poly(lactic-co-glycolic) acid–encapsulated microparticles improves pulmonary hypertension. J Am Heart Assoc. 2021;10:e019091Simultaneous Pharmacologic Inhibition of Yes-Associated Protein 1 and Glutaminase 1 via Inhaled Poly(Lactic-co-Glycolic) Acid–Encapsulated Microparticles Improves Pulmonary Hypertension. [PubMed: 34056915]

Author Manuscript Author Manuscript Author Manuscript Author Manuscript

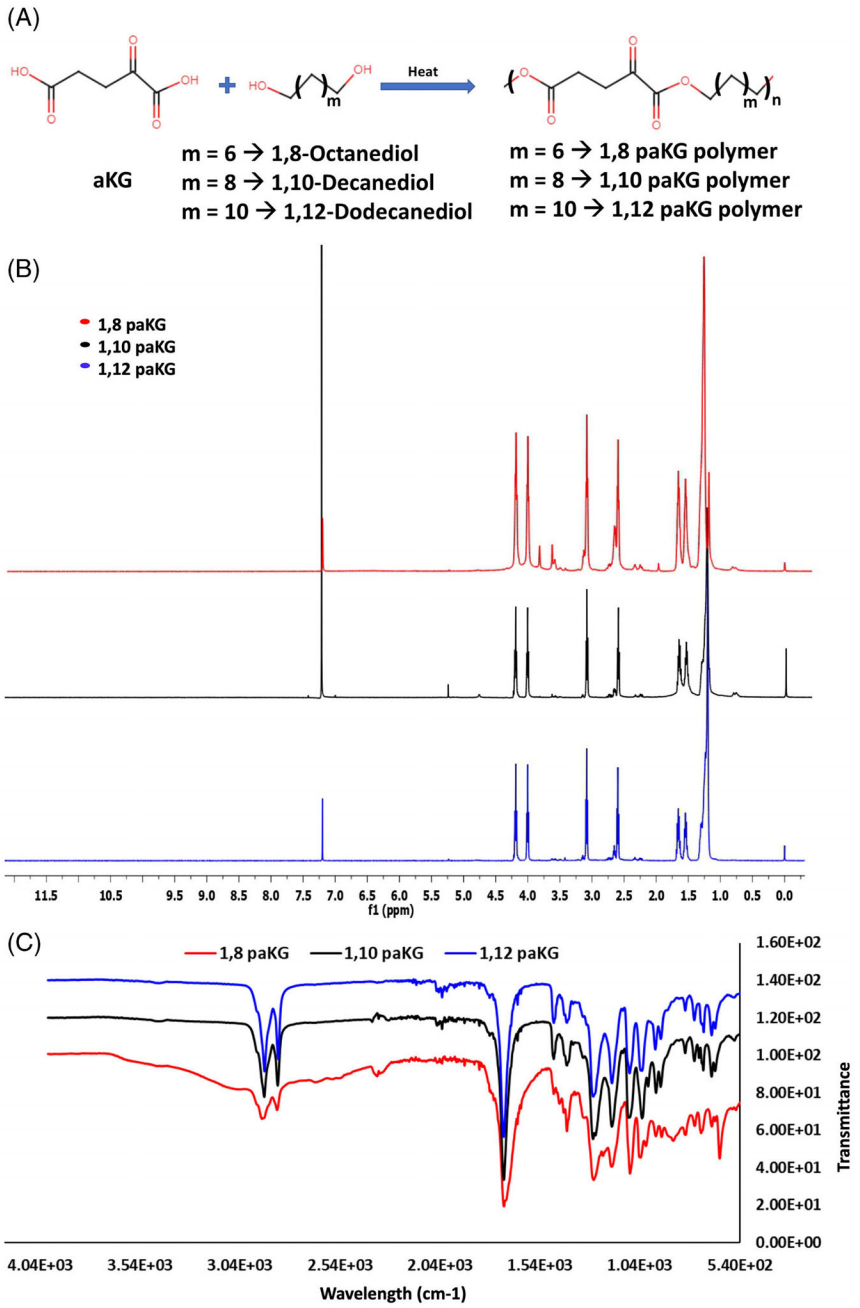

FIGURE 1.

Synthesis of paKG polymers. (A) Schematic for preparation of paKG polymers. (B) ^{1}H NMR of synthesized paKG polymers using $CDCl_3$ as a solvent. (C) FT-IR spectrum for the functional groups present on the polymers.

Author Manuscript Author Manuscript Author Manuscript Author Manuscript

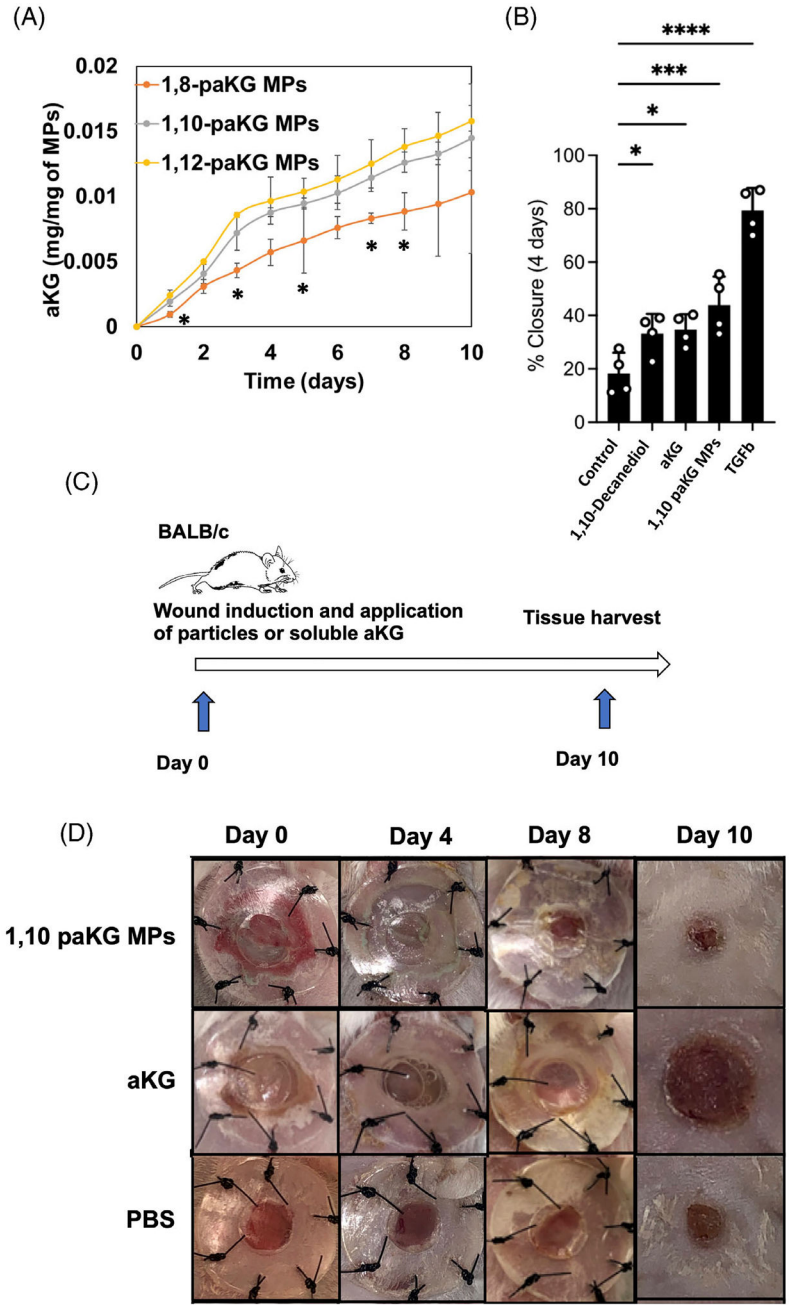

FIGURE 2.

paKG MPs facilitate faster wound closures in vitro and in vivo. (A) Release kinetics of aKG was performed from the microparticles generated from different polymers ($n = 3$, avg ± SD, *$p < .05$ significance of 1,8-paKG MPs as compared to 1,10-paKG MPs and 1,12-paKG MPs, Student's T test). (B) Percentage closure of the wound (scratch assay in HaCaT human keratinocyte cells in vitro) was quantified on day 4, which demonstrates that 1,10-paKG MPs were able to decrease the wound area significantly higher than the PBS control ($n = 4$, avg ± SEM, *$p < .05$, One-way ANOVA). (C) In vivo study design. (D) Representative images of the wound after treatment with 1,10-paKG microparticles demonstrate faster

wound healing as compared to the other groups. (Note – the dark region represents scab and closed wound in 1,10-paKG microparticles group) ($n = 6$, avg ± SEM, $*p < .05$).

Author Manuscript Author Manuscript Author Manuscript Author Manuscript

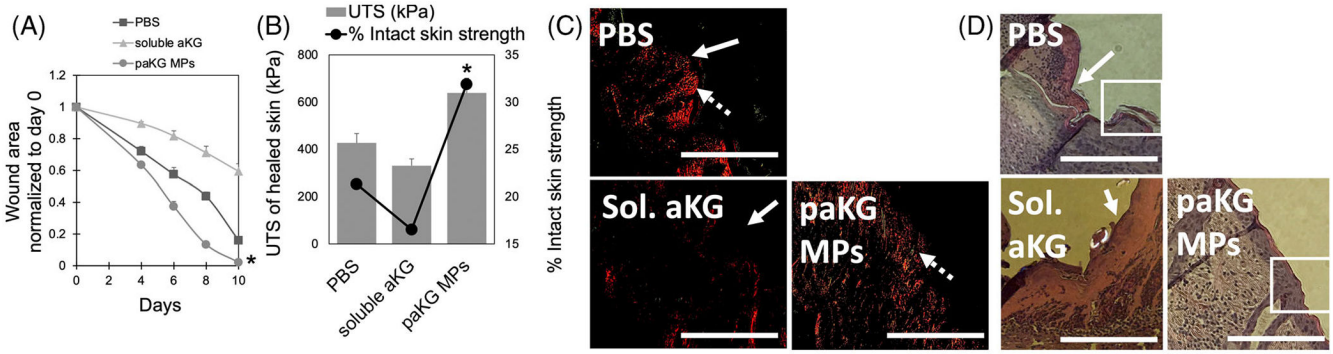

FIGURE 3.

Treatment with paKG MPs results in faster wound closure and higher ultimate tensile strength (UTS). (A) The wound area (normalized to day 0) is shown, which demonstrates that the 1,10-paKG microparticles close the wound within 10 days ($n = 6$, avg ± SEM, $*p < .05$, significantly different than all other groups, One-way ANOVA). (B) The ultimate tensile strength (UTS) and % strength as compared to the intact skin was found to be highest for 1,10-paKG microparticles and lowest for soluble aKG group on day 10 ($n = 6$, avg ± SEM, $*p < .05$, significantly different than all other groups). (C) Picrosirius staining performed on the skin tissue isolated from the wound bed demonstrated that the paKG MPs allowed for deposition of collagen type III (green, dashed arrow) and collagen type I (red, solid arrow) in the tissue (scale bar = 330 μm, $n = 3$ mice per group, 3 technical replicates). (D) H&E performed on the skin tissue isolated from the wound bed demonstrated that the paKG MPs decreased immune cell infiltration in the wound bed.

Author Manuscript Author Manuscript Author Manuscript Author Manuscript